Pockets of Open Cells (POCs) and Drizzle in Marine Stratocumulus

Bjorn Stevens[1*], Gabor Vali[2], Kimberly Comstock[3] Robert Wood[3],
Margreet C. van Zanten[1,4], Philip H. Austin[5], Christopher S. Bretherton[3], Donald H. Lenschow[6]
[1]Department of Atmospheric Sciences, UCLA, Los Angeles, CA, 90095, USA.
[2]Department of Atmospheric Science, University of Wyoming, Laramie, WY, 82071, USA.
[3]Department of Atmospheric Sciences, University of Washington, Seattle, WA, 98195, USA.
[4] Institute of Marine and Atmospheric Research Utrecht, Utrecht University, The Netherlands
[5]Atmospheric Sciences Programme, University of British Columbia, Vancouver BC, V6T 1Z4, Canada.
[6]National Center for Atmospheric Research, Boulder CO, 80307, USA.
[*]To whom correspondence should be addressed; E-mail: bstevens@atmos.ucla.edu.

Data from recent field studies in the northeast and southeast Pacific are used to investigate pockets of open cells (POCs) embedded in otherwise uniform stratocumulus. The cellular structure within a POC resembles broader regions of open cellular convection typically found further offshore. In both regions, cells are comprised of precipitating cell walls and cell interiors with depleted cloud water, and even clearing. POCs are long lived and embedded in broader regions of stratocumulus where average droplet sizes are relatively large. In contrast, stratiform, or unbroken, cloud formations tend to be accompanied by less, or no, drizzle suggesting that precipitation is necessary for the sustenance of the open cellular structure. Because, by definition, open cells are associated with a reduction in cloud cover these observations provide direct evidence of a connection between cloudiness and precipitation—a linchpin of hypotheses which posit a connection between changes in the atmospheric aerosol and cli-

mate.

A curious feature of the cloud climatology over regions of the globe where low-lying marine stratiform clouds predominate is the appearance of pockets of seemingly cloud-free air embedded in an otherwise homogeneous cloud field. The irregularities in the cloud field as seen in the visible satellite imagery in the left and upper panels of Fig. 1 are an example of such features. Here two elongated regions of very low reflectivity stripe the southern portion of the cloud field, with more irregular pockets evident in the eastward extension of these low-reflectivity bands. Because factors which regulate the reflectivity of low clouds can critically affect the climate system as a whole (*1*,*2*), features such as these are not simply curious; they may also provide clues into the processes which regulate cloudiness on larger scales, and thus climate.

Upon closer examination such low reflectivity pockets or bands are rarely completely clear; instead they evince an underlying patterning reminiscent of open cellular convection (*3*). In Fig. 1 hints of this patterning are most evident in the westward extension of the bands. For this reason, and because the envelope of open cells can adopt myriad geometries, hereafter we refer to such features as pockets of open cells (POCs). By looking at $\Delta T_{B,}$ the 11 minus 4 μm brightness temperature, POCs can also be detected in the night-time satellite imagery. This is shown in the right and bottom panels of Fig. 1 which show that these POCs are long lived, and are embedded in regions of relatively small values of $\Delta T_{B,}$ indicative of larger cloud droplets (*4*), and more precipitation (*5*). Along with the tendency to display an underlying cellular structure, both of these latter characteristics are generic features of the many other examples of POCs we have found in the satellite record. Because the shapes and sizes of POCs vary considerably (*6, 7*), very large pockets with pronounced cellular patterning might be better described simply as regions of open cellular convection.

The idea that POCs are simply compact regions of open cellular convection merits asking whether, in addition to the cellular patterning, there are other features of open cellular convec-

tion which share characteristics we have attributed to POCs (e.g., longevity and an association with larger droplets or more precipitation)? To answer this we analyze data collected as part of the recent EPIC field study (*8*) in which a boundary between a region of open and closed cellular convection advected over the NOAA Research Vessel the *Ronald H. Brown* (see Fig. 2). Here the microphysical structure of the cloud fields is investigated with the help of an upward pointing cloud radar, whose measurements of reflectivity are contoured in time-height space at the bottom of Fig. 2. The analysis shows that when the region of open cellular convection is overhead, the cloud field has a more cellular structure, with frequent periods of radar reflectivities (a proxy for drizzle, *9*) extending to the surface. In the region to the south (which was sampled by the ship after 0900 local time and is better characterized as closed cellular convection) radar reflectivities were considerably smaller and the cloud field appeared more homogeneous. Interpretation of this data is complicated by the diurnal cycle and the absence of *in situ* cloud data, but it supports the idea that regions of open cellular convection are characterized by cloud fields more conducive to precipitation, and that the boundaries between the different modes of convection are coherent over long periods of time.

These data raise the question as to whether POCs (and by inference open cells) are initiated, and/or maintained by drizzle. If so this would provide empirical support for a hitherto untested assumption underlying a class of hypotheses relating changes in the atmospheric aerosol to patterns of cloudiness, namely that precipitation is associated with a reduction in cloudiness (*10,11,12*). It could also provide a means for remotely tagging precipitating regions of the boundary layer cloud field (*13*).

To help answer this question we analyze a POC serendipitously sampled during the second research flight (RF02) of the DYCOMS-II field study (*14*). Fig. 3 shows the morning visible satellite imagery and reflectivity from a downward looking airborne cloud radar. In the satellite imagery the POCs appear to be localized extensions of broader regions of open cellular con-

vection to the west — reinforcing the connections discussed above. More strikingly the radar data shows that the POC is comprised of mesoscale cells whose walls are loci of intensified convection, with locally higher cloud tops, and radar backscatter (i.e., drizzle) extending to the sea-surface. Cell interiors have locally lower cloud tops and even regions of complete clearing. Because the lidar, unlike the radar, is sensitive to even trace amounts of cloud, the clearings in Fig. 3 are best identified by regions where the lidar pulse penetrates to the surface. As was evident in the EPIC data, more overcast regions in the satellite imagery are associated with more uniform clouds with little or no precipitation (*15*). This provides the strongest evidence yet that regions of open cellular convection are coincident with precipitating regions of the flow.

In situ measurements allow us to be more quantitative. In Fig. 4 we show data from two additional flight periods from just before sunrise. For orientation, both flight legs are overlaid on the ΔT_B field as derived from GOES (*16*). Despite the degradation by the relatively coarse (4km) resolution of the satellite image, the region of the POC is still evident in the envelope of near zero values of ΔT_B. As in Fig. 1 the POCs in the vicinity of RF02 are embedded in a broader cloud field characterized by relatively small values of ΔT_B, or large droplets (*17*). Data from both flight periods are shown as time-series in the Figure: the northern flight-leg was flown near the surface (100m) in a clockwise direction and bisected the POC during the first 900s of the time-series (shown in upper panel); the southern leg was flown in a counter-clockwise fashion approximately 400 m above cloud top, crossing over the POC near the middle of the leg. The liquid-water content q_l from the northern track and the reflectivity from the southern track reinforce the idea that POCs delineate regions of locally enhanced precipitation. By using the *in situ* data to calibrate local rain-rate reflectivity relationships we can estimate mean surface precipitation rate from the radar to be around 1 cm d^{-1} within the precipitating cell walls of the POC, which is more than twice as large as the surface evaporation rate. Cloud base rain-rates are two to threefold larger yet (*18*). Precipitation rates of this magnitude are thus rapid enough

to deplete the cloud of all its liquid water in 15-30 minutes (*19*). The persistence and apparent coherence of these vigorously precipitating regions suggest that the open cells are relatively stable flow configurations which organize to maintain the moisture supply to the precipitating cell boundaries. Circulations capable of such transport are consistent with the observation that envelopes of enhanced radar reflectivity tend to have locally elevated cloud tops.

The cellular structure of the POC is particularly evident in the *in situ* near-surface measurements of the northern flight leg. Here the quasi-periodic envelopes of precipitation are associated with sharp increases in the total water mixing ratio, and reduced values of the temperature — mini-cold pools driven by the evaporation of precipitation in the sub-cloud layer (*20*). Unlike the cold pools of deep precipitating convection, the moisture enhancement in the precipitating regions more than offsets the temperature perturbations. These structures are in marked contrast to the flow far from the POC, where the boundary layer thermodynamic structure is more uniform, and there is no evidence of surface precipitation. Although it is difficult to discern the detailed dynamics of the circulations in the vicinity of the cells from these data, the emergence of cells supports previous theoretical work (*21-22*) that argues precipitation from initially stratiform clouds drives a more diabatic, cumulus-like circulation, characterized by narrower regions of convective ascent and broader regions of stabilized descent.

One puzzling aspect of the near-surface data is the tendency for the boundary layer to be moister and richer in CN within the vicinity of the POC. Normally precipitation would be expected to dry the boundary layer (at least away from the evaporating shafts or precipitation), and, in the absence of new particle formation, remove condensation nuclei from the air. However, the air directly above the POC was also more humid and aerosol laden, both of which are consistent with the otherwise counter-intuitive nature of the near-surface data. The moist layer capping the cloud in the vicinity of the POC reduces the rate of entrainment drying thereby deepening the cloud and augmenting precipitation. This may explain why the POC formed and

why it is more localized than the region of large cloud droplet sizes seen in Fig. 4. Similar correlations have been noted in past field studies, but were not apparent in the EPIC data. That said, this influence is relatively weak making it difficult to argue quantitatively given other confounding effects (*24*). Nonetheless, the presence of a distinct character to the thermodynamical structure of the flow directly above the POC does suggest that either the POC is induced by such features, or that both the POC and the overlying thermodynamic structure were imprinted by some other process — perhaps sometime in the past.

In summary, data from two recent field experiments in the northeast and southeast Pacific stratocumulus regions suggest that coherent, long-lived, pockets of open cellular convection are coupled to the development of precipitation (*24)*. These findings are consistent with theoretical work that suggests that the transition to more strongly precipitating flows should induce such a cloud transition. Because such features are readily identified in satellite imagery they could facilitate attempts to develop drizzle climatologies using satellite observations as well as serve as natural laboratories for investigating the interactions among cloud dynamics, precipitation and properties of the atmospheric aerosol.

References and Notes

1. A frequently cited figure is that a 4% reduction in the albedo of low clouds could offset the expected warming due to greenhouse gases. D. A. Randall, J. A.Coakley, Jr., C. W. Fairall, R. A. Kropfli, and D. H. Lenschow, *Bull. Amer. Meteorol. Soc.,* **65,** 1290, (1984).

2. Ma, C.-C. and C. R. Mechoso and A. W. Robertson and A. Arakawa, *J. Clim.*, **9**, 1635, (1996).

3. Open cellular convection is characterized by irregular cellular patterns with cell boundaries having a large albedo and cell interiors having relatively lower albedos, e.g., E. M. Agee, *Bull. Amer. Meteorol. Soc.*, **65**, 938, (1984).

4. For instance, a change in ΔT_B of several Kelvin can be accounted for by a reduction in the cloud optical depth from values of 15 to unity (which is not consistent with the visible imagery), or by changes in the effective radius from 6 to 12 μm for a cloud with a fixed optical depth of 15, e.g., Fig. 1 of J.C. Perez *et al., J. Rem. Sensing of Environ.,* **73,** 31, (2000).

5. The idea that precipitation correlates with droplet size is the basis of many satellite retrievals, and is supported by *in situ* measurements from a variety of field campaigns, e.g., Hermann Gerber, *J. Atmos. Sci* **53,** 1649 (1996).

6. Similar features are sometimes called cloud polynya, actinae, rifts and hybrid cells among other things. See A. F. Krueger and S. Fritz, *Tellus* **13**, 1, (1961) for an early discussion of similar features.

7. A recent survey of POC-like features based on modern high-resolution satellite images is provided by Garay and Davies, *Proceedings of the Seventh International Conference on Southern Hemisphere Meteorology and Oceanography,* American Meteorological Society, Boston MA, (2003).

8. EPIC (Eastern Pacific Investigations of Climate), C. S. Bretherton, *et al., Bull. Amer. Meteorol. Soc.,* submitted.

9. At 95 Ghz the radar reflectivity is sensitive to the sixth power of cloud droplet diameter — high radar reflectivities accentuate regions of larger droplets, and hence precipitation, e.g., G. Vali, R. D. Kelly, J. French, S. Haimov, D. Leon, R. E. McIntosh and A. Pazmany, *J. Atmos. Sci.* **55**, 3540, (1998).

10. Albrecht, B. A., *Science* **245,** 1227 (1989).

11. D. Rosenfeld, *Science* **287,** 1793 (2000).

12. See U. Lohmann and G. Lesins, *Science* **298,** 1012 (2002), for a recent attempt at quantifying this effect.

13. Currently such estimates are made by estimating the cloud-droplet effective radius using daytime satellite data, e.g., Q. Han, W. Rossow, R. Welch, A White, and J. Chou, *J. Atmos. Sci* **52,** 4183 (1995).

14. DYCOMS-II (the second dynamics and chemistry of marine stratocumulus study), B. Stevens, *et al., Bull. Amer. Meteorol. Soc.,* **84**, 579, 2003)

15. These patterns are particularly evident in flight-by-flight comparisons of the DYCOMS-II data, where the tendency for enhanced drizzle correlates with the appearance of more evident cellular structure and larger-cloud droplets as measured by ΔT_B, M. C. van Zanten, B. Stevens, G. Vali and D. Lenschow in preparation

16. In this Figure, the flight tracks were advected to a position valid at 06:15 local time, coincident with the time of the satellite image. This is approximately 15 minutes after the first flight track and 15 minutes before the southern flight segment. The advection of the flight tracks allows the method presented in Stevens, B., D. H. Lenschow, I. Faloona, C.H. Moeng, D. K. Lilly, B. Blomquist, G. Vali, A. Bandy, T. Campos, H. Gerber, S. Haimov, B. Morley, D.C. Thornton, *Quart. J. Roy. Meteor. Soc.,* **129,** 1, (2003).

17. Droplet concentrations during RF02 were among the lowest of all flights, averaging about 60 cm^{-3}.

18. To estimate the surface and cloud base rain-rates, *in situ* data from two independent probes, a 260X and a 2D-C, were used to calibrate reflectivity rain-rate relationships for each flight and for each flight-level, M. C. van Zanten, B. Stevens, G. Vali and D. Lenschow in preparation. The redundant instrumentation, and extensive sampling allowed the first comprehensive survey of drizzle in this climatologically important cloud deck. Error estimates yield a one-sigma uncertainty in the net drizzle rates is about 30% of the mean.

19. Our estimate of a cloud depletion time-scale is based on estimates of cloud liquid water path of 0.15 mm (corresponding to a cloud of approximately 450m thick with a cloud top liquid water contents of 0.6 g kg^{-1}).

20. Similar structures in the vicinity of precipitating shallow convection have been observed in the past, e.g., Jensen, J.B., and S. Lee and P. B Krummel and J. Katzfey and D. Gogoasa, *Atmos. Res.*, **54,** 117 (2000).

21. J. Bjerknes, *Q. J. Roy. Meteorol. Soc.,* **64,** 325 (1938).

22. B. Stevens, W. R. Cotton, G. Feingold, C-H. Moeng, *J. Atmos. Sci.* **55**, 3616, (1998) used large-eddy simulation to show that a variant of the above-cited argument by Bjerknes seems to explain the cloud transition when precipitation becomes active in stratocumulus.

23. In the absence of other effects, given entrainment rates similar to those analyzed for RF01, *(reference cited in 16)* an increase in the humidity of the air above the boundary layer from 2 to 5 g kg^{-1} would lead to a 0.5 g kg^{-1} difference in the boundary layer humidity over a period of 10 hours. Such an increase in relative humidity within the boundary layer would double the liquid water path of the cloud. However, confounding effects such as the apparent reduction in the stability of the free troposphere just above the POC, and reduced downward long-wave radiation above the POC (not shown) complicate this argument.

24. In retrospect, measurements from June 30th flight of the First International Satellite Climatology Project Regional Experiment (cf., Figs. 1 and 7 of P. Austin, Y. Wang, R. Pincus and V. Kujala, *J. Atmos. Sci., 52,* 2329 1995) also provide a vivid corroboration of the points being made here.

This research was supported by the NSF through grants ATM-0097053, ATM-0094956, ATM-0082384, and its support of the National Center for Atmospheric Research, as well as through funding by NSERC/CFCAS, ONR (through the EPSCoR program, NASA grants NAGS5-10624, NAG 5-12559, the Nederlandse Organisatie voor Wetenschappelijk Onderzoek and an NDSEG fellowship.

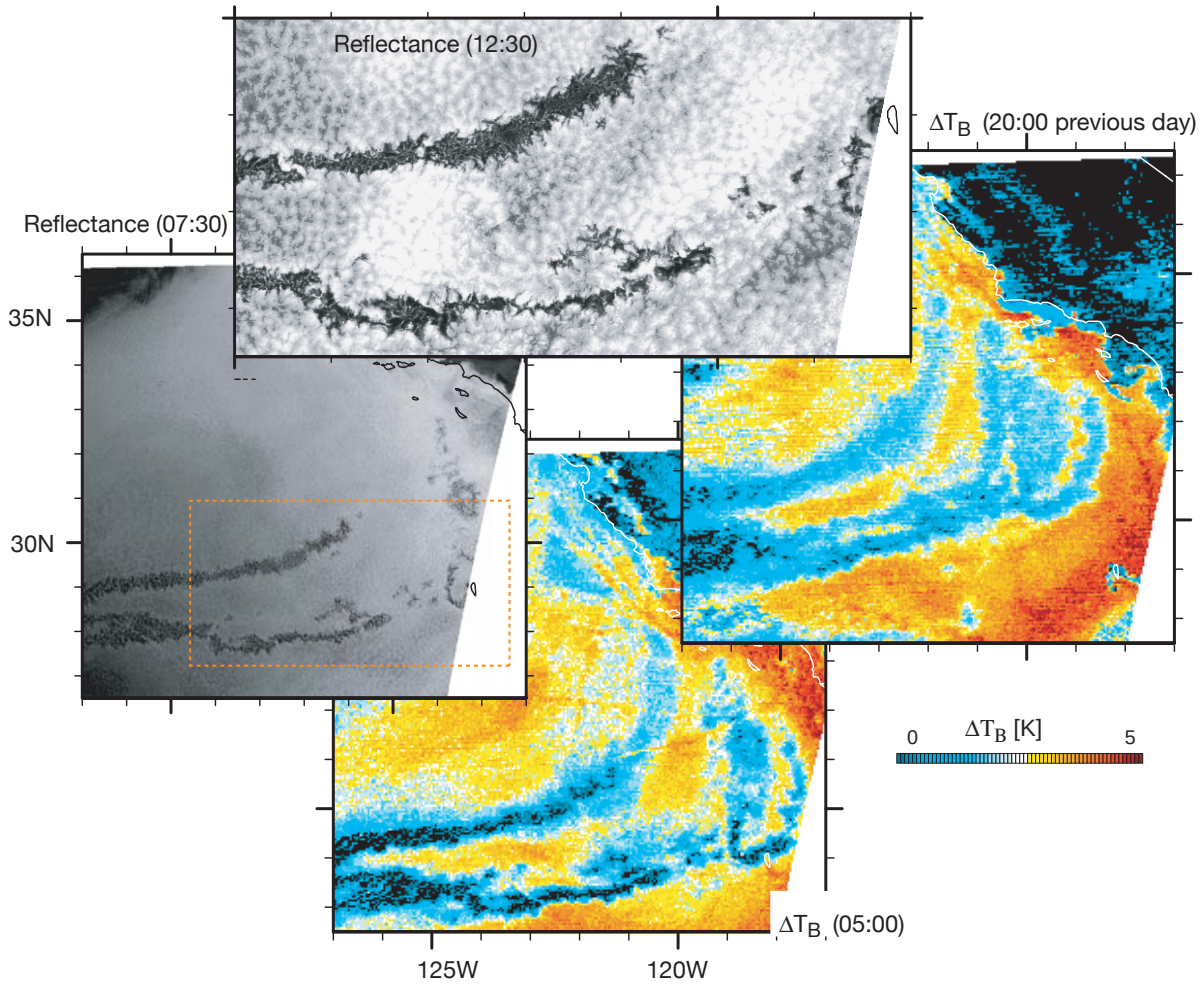

Figure 1: Sequence of images of the North-East Pacific on July 27, 2001 constructed from GOES-10 data. The color images are differences between channels four and two of GOES, while the grey-scale image is cloud albedo as measured by channel 1 radiances. The visible image has a pixel size of 1 km, in contrast to the 4km pixel of the infrared imagery.

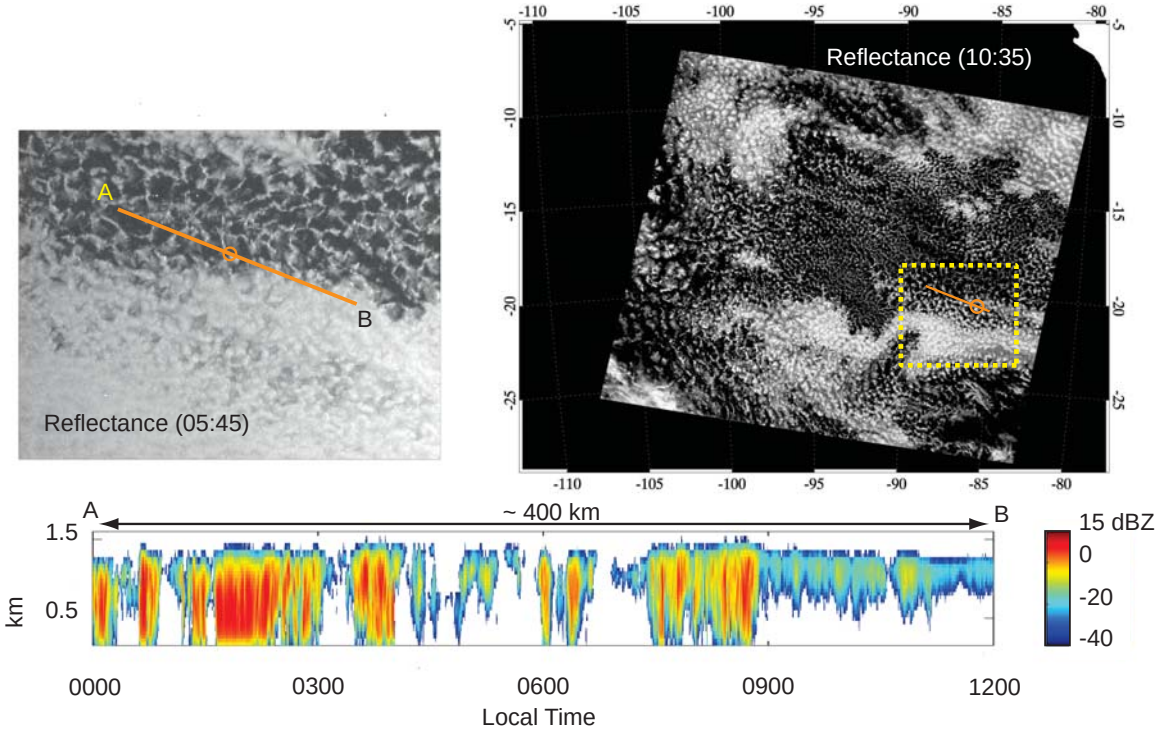

Figure 2: Upper left panel: Channel 1 reflectance from the southeast Pacific from GOES 8. The upper right panel shows the pseudo reflectance as measured by MODIS. All times are local time. The radar reflectivity data is taken from an upward pointing cloud radar operated from the the NOAA RV *Ron Brown* which was on station at 85W, 20S as part of the EPIC experiment. In each satellite image the position of the *Ron Brown* is indicated by the orange open-circle marker, and the approximate trajectory of the cloud field, as estimated from surface wind measurements is indicated by the orange line.

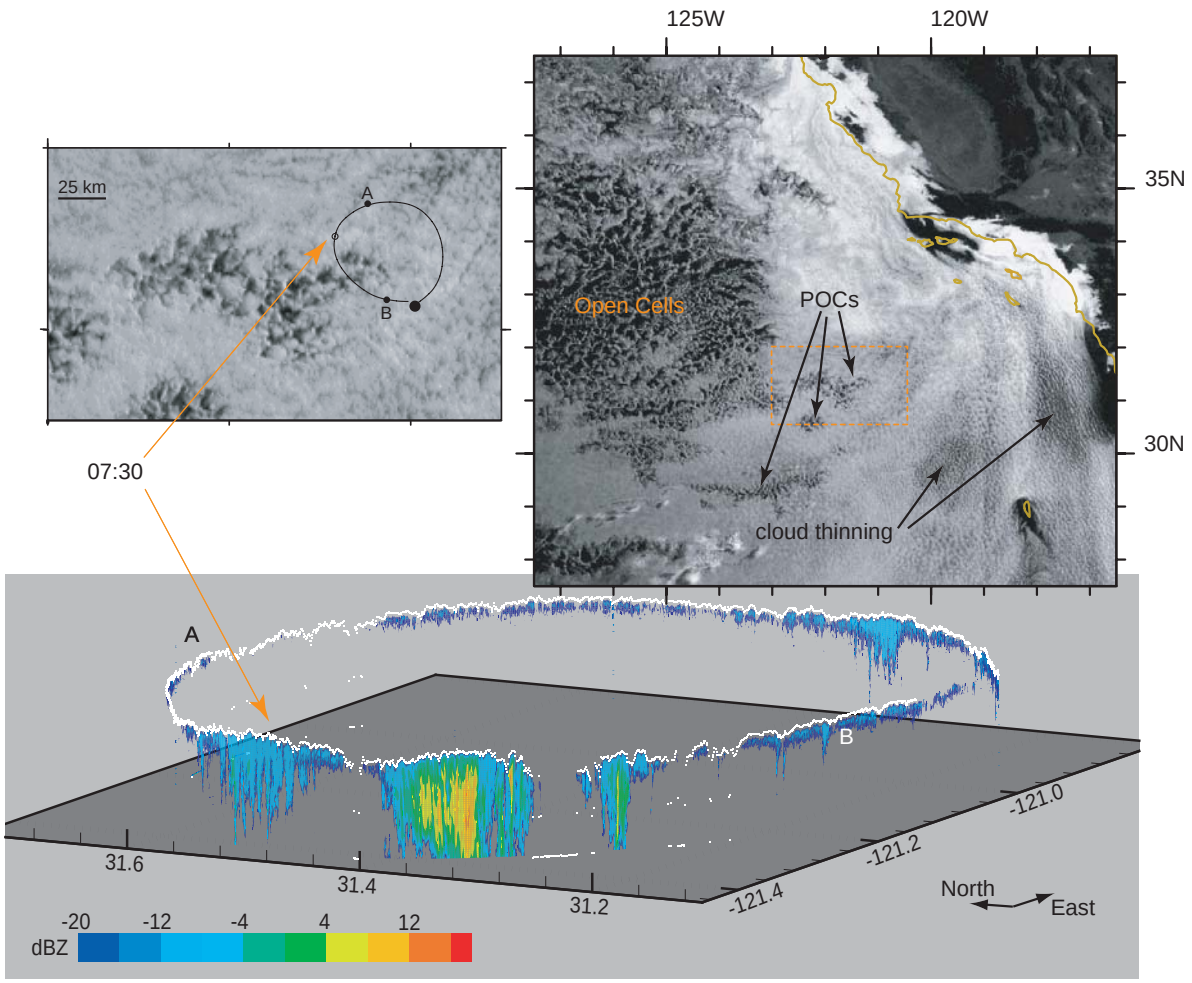

Figure 3: Upper right panel: Channel 1 reflectance over the northeast Pacific from GOES-10 at 0730 local time (14:30 UTC) for July 11, 2002. Upper left panel: zoomed image of reflectance field from boxed region in regional image, overlaid on this image is a flight segment from RF02 which spans the time of the over-pass and from which radar and lidar data is presented in lower panel. The zoomed image highlights a tilde-shaped POC boxed in the upper left image. Lower panel: time height radar reflectivities filled, with cloud top height as estimated by downward looking lidar shown by white line. Regions where lidar detects no cloud are shown by a lidar trace at the surface. The time for which the satellite image is valid is indicated on the flight tracks.

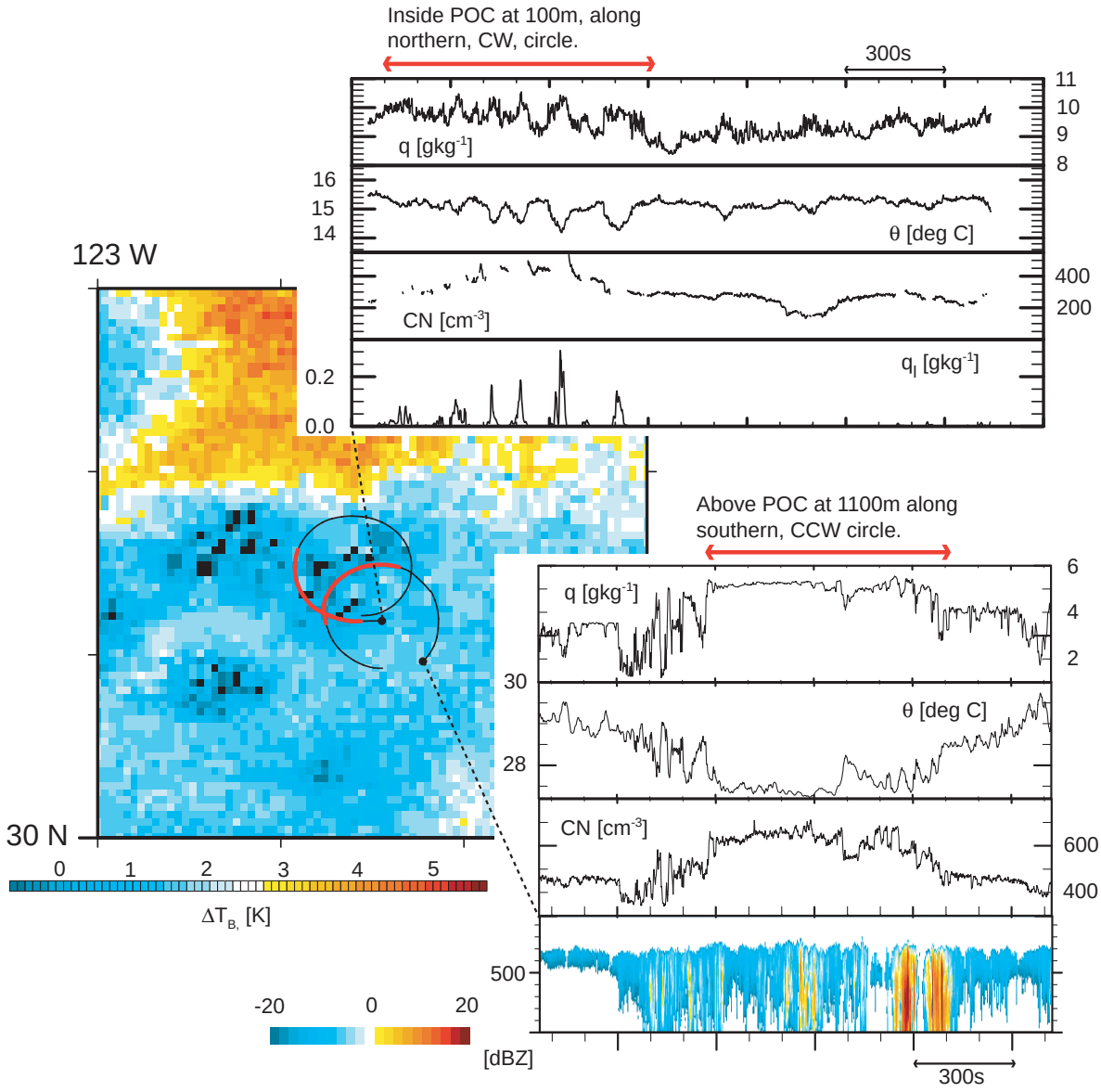

Figure 4: ΔT_b as measured from GOES 10 is contoured on left, with superimposed flight circles for the boxed tilde-shaped POC in Fig. 2. The part of the flight circle which, roughly speaking, is over (or in) the POC is indicated with red. The starting point for each circle is denoted by a black dot, thus the northern circle was flown in a CW fashion, and the southern circle in a CCW fashion. Time-series data for the northern and southern circles are plotted in upper and lower panels respectively. They show from top to bottom: water vapor mixing ratio (q) as measured by a Lyman-α probe, potential temperature (θ), condensation nuclei (CN). The bottom panel is the liquid water (q_l) for the northern circle and the radar reflectivity for the southern circle. The CN measurements are corrupted in the presence of rain, and thus are set to missing value when measurable drizzle is evident.